Published in final edited form as:
Br J Ophthalmol. 2009 September ; 93(9): 1223–1227. doi:10.1136/bjo.2008.150110.

Reconstructing foveal pit morphology from optical coherence tomography imaging

A M Dubis[1], **J T McAllister**[2], and **J Carroll**[1,2,3]

[1]Department of Cell Biology, Neurobiology, & Anatomy, Medical College of Wisconsin, Milwaukee, Wisconsin, USA

[2]Department of Ophthalmology, Medical College of Wisconsin, Milwaukee, Wisconsin, USA

[3]Department of Biophysics, Medical College of Wisconsin, Milwaukee, Wisconsin, USA

Abstract

Aim—The aim of this study was to describe an automated method for extracting quantitative measures of foveal morphology from optical coherence tomography (OCT) images of the human retina.

Methods—We performed a methodological study and retrospective investigation of selected cases. Sixty-five human subjects were included: 61 healthy subjects and four female carriers of blue-cone monochromacy (BCM). Thickness data from B-scans traversing the foveal pit were fitted to a mathematical model designed to capture the contour of the foveal surface. From this model, various metrics of foveal morphology were extracted (pit depth, diameter and slope).

Results—Mathematical descriptions of foveal morphology enabled quantitative and objective evaluation of foveal dimensions from archived OCT data sets. We found a large variation in all aspects of the foveal pit (depth, diameter and slope). In myopes and BCM carriers, foveal pits were slightly less deep and had a more shallow slope, although these differences were not significant.

Conclusions—Offline analysis of OCT data sets enables quantitative assessment of foveal morphology. The algorithm works on the Stratus™ and Cirrus™ macular thickness protocols, as well as the Spectralis® and Bioptigen© radial-line scan protocols, and can be objectively applied to existing data sets. These metrics will be useful in following changes associated with diseases such as retinopathy of prematurity and high myopia, as well as in studying normal postnatal development of the human fovea.

The fovea is characterised by an avascular zone, a marked increase in cone packing and an excavation of inner retinal neurons.[1] While the site of the human fovea can be identified as early as 22 weeks gestation,[2] foveal development is not complete until 4 to 7 years after birth.[3] The fovea occupies a rather small retinal area. However, some 25% of retinal ganglion cells sample the foveal cone mosaic.[4] Given the importance of central vision, characterising foveal structure in normal and diseased retina is of great interest. Previous

Correspondence to: Dr J Carroll, Medical College of, Wisconsin, The Eye Institute, 925 N. 87th Street, Milwaukee, WI 53226, USA; jcarroll@mcw.edu.

Competing interests: None declared.

Ethics approval: The study followed the tenets of the Declaration of Helsinki and was approved by the Medical College of Wisconsin Institutional Review Board.

Patient consent: Obtained.

Provenance and peer review: Not commissioned; externally peer reviewed.

work has revealed considerable variation in foveal characteristics of the normal retina, such as avascular zone diameter,[5] peak cone density[6] and rod-free zone diameter.[3] The most prominent feature of the fovea is the pit itself, although little attention has been paid to describing the contour of the foveal surface. Williams (1980) used psychophysical techniques to derive an estimate of the foveal slope in four individuals, and found that the foveal slope was 43° at 150 μm eccentricity.[7] Hammer *et al* (2008) used optical coherence tomography (OCT) to subjectively measure foveal pit depth in normal subjects and individuals with retinopathy of prematurity, and reported some variability in pit depth, although there were only five normal subjects.[8] Quantitative and objective measurements of pit morphology from a large population of normal retinas would enhance our ability to use these metrics to study foveal morphology in various retinal disorders; normative data in this regard could be used to constrain models of foveal development.[9–11]

OCT provides exquisite views of foveal architecture in the living retina. Clinical OCT devices provide a variety of real-time information to the user regarding the macular region. However, there is no automated and quantitative description of foveal pit morphology currently available. We imaged 130 eyes and developed an automated algorithm to extract morphological characteristics of the foveal pit (slope, depth and diameter) from standard OCT scan data sets, both time-domain and spectral-domain.

MATERIALS AND METHODS

Subjects

Thirty-nine emmetropic, 22 myopic and four female carriers of blue-cone monochromacy (BCM) were recruited for this study. The myopic group consisted of individuals with a refractive error of greater than –3 D. None of the eyes showed any gross signs of ocular disease, and both eyes were imaged in each individual. Subjects ranged in age from 13 to 52 years, with a mean of 26.3 years.

Imaging

Sixty-four subjects were imaged using a Zeiss Stratus™ OCT3, and 21 of these subjects and one of the BCM carriers were imaged with a Zeiss Cirrus™ HD-OCT (Carl Zeiss Meditec, Dublin, California, USA). One subject was also imaged with the Bioptigen SD-OCT (Bioptigen, Durham, North Carolina, USA) and the Spectralis HRA+OCT (Heidelberg Engineering, Vista, California, USA). The fast macular thickness retinal volumetric ("fast mac") scan was used on the Stratus. The nominal lateral scan length was 6 mm,[i] the standard setting for the fast mac protocol. Each fast mac scan set consists of six B-scans (at 128 A-scans/B-scan), taken at 30° intervals. Retinal thickness files (.rth) for each fast mac data set were imported into custom MatLab (Mathworks, Natick, Massachusetts, USA) analysis software using the export feature in the Zeiss software. On the Cirrus, we acquired macular volume data sets using the standard 6 mm × 6 mm scan set (512 A-scans/B-scan; 128 B-scans). Retinal thickness values, from the inner limiting membrane (ILM) to the retinal pigment epithelium (RPE), were exported into MatLab, and a simulated scan set analogous to the Stratus fast mac scan set was created by extracting six radial lines separated by 30°, thus allowing a direct comparison between modalities. The data were obtained using the Cirrus Research Browser (Carl Zeiss Meditec), an off-instrument review software package. The browser allows export of calculated data that are otherwise displayed graphically or in a table with the standard instrument analysis modules. On the Bioptigen (1000 A-scans/B-scan) and Spectralis (1024 A-scans/B-scan) we also used a radial scan

[i]Scans for each subject were corrected for inter-individual differences in axial length based on Leung et al (2007).[12] Axial length in our subjects ranged from 21.44 to 27.5 mm; thus, actual scan lengths ranged from 5.26 to 6.75 mm.

profile, consisting of six radial lines (B-scans) separated by 30°. Images were exported and the ILM and RPE were manually segmented using ImageJ (www.rsb.info.nih.gov/ij/) to compute retinal thickness.

Assessing pit morphology

Model fit—The contour of the foveal pit is well represented by a Gaussian function.[7] However, while this function approximates the shape of the foveal pit, it does not completely capture the rim contour. It is identification of the rim contour that provides access to the automated measure of pit depth and diameter. We tested several functions for their ability to fit foveal pit contour, and found that a difference of Gaussians (DoG) function (equation 1) provides the best fit to the foveal OCT scans. In this model, μ_1 and μ_2 serve as the means of the respective Gaussian functions, σ is the standard deviation, and x is the x-coordinate location within the scan. It is important to note that although μ_1 and μ_2 are not mathematically linked, in our model they are required to be equal to enable automated modelling of pit morphology and extraction of foveal pit parameters. Raw data for retinal thickness were fitted to the DoG (equation 1) using least squares analysis.

$$F(x)=A_1\times\left(\exp\left(\frac{(x-\mu_1)^2}{-2{\sigma_1}^2}\right)\right)-A_2\times\left(\exp\left(\frac{(x-\mu_2)^2}{-2{\sigma_2}^2}\right)\right)+z \quad (1)$$

Figure 1A shows the raw thickness values for the six B-scans from a fast mac scan set for one subject, while fig 1B shows the DoG fits to the individual B-scans. One of the problems with reconstructing foveal volumes from time-domain OCT is eye movement. Even in individuals with superior fixation stability, small saccades occur that can disrupt the ability to automatically model the pit contour. Thus, aligning scans from within the fast mac data set is an important first step in reconstructing foveal morphology. Using the DoG mean (μ_1 and μ_2 in equation 1), we approximate the lateral shift for each scan, relative to an arbitrary centre. We then shift each scan to align to this common centre, as would be expected in the ideal observer case where there is no fixational eye movements and all scans pass through the foveal centre. This correction only accounts for lateral movement of the eye between scans in the fast mac scan set. Determining the shift of each scan allows implementation of an automated way to reject scan sets with too much eye movement, which would impair our ability to model the pit contour reliably. Thus, if any scan had a shift larger than 0.3 mm, the entire fast mac set was not used. This was an empirically derived threshold, and could be modified depending on the experiment. Figure 1C shows the result of the corrective shift applied to the six B-scans.

Extracting foveal pit parameters—In order to extract the various foveal pit metrics (diameter, depth and slope) automatically, we calculated the first derivative of the DoG fits for each of the six B-scans in each fast mac scan set. Figure 2 shows a typical B-scan from the Stratus fast mac scan set, and the exported thickness values and DoG model fit (middle panel).

$$F'(x)=A_1\times\left(\left(\frac{(x-\mu_1)}{{\sigma_1}^2}\right)\exp\left(\frac{(x-\mu_1)^2}{-2{\sigma_1}^2}\right)\right)-A_2\times\left(\left(\frac{(x-\mu_2)}{{\sigma_2}^2}\right)\exp\left(\frac{(x-\mu_2)^2}{-2{\sigma_2}^2}\right)\right) \quad (2)$$

To identify anatomical landmarks within the scan, we examine the first derivative $F'(x)$ of the DoG fit (equation 2 and fig 2, bottom panel). There are five key points of interest on this curve: points A and E indicate the peak of the foveal rim, as the slope of the foveal contour is zero at these locations. Likewise, point C has a zero slope, and this marks the centre of the

pit. Finally, points B and D identify the points of maximum slope on either side of the foveal centre. From these five landmarks, we can extract three prominent features of the foveal pit —diameter, depth and slope. We define diameter as the distance from rim to rim,[113] illustrated in fig 2 as the distance between points A and E. The measured values of diameter for each eye are an average of the measured diameter of each of the six B-scans in the fast mac scan set.

The depth of the foveal pit is defined as the difference between retinal thickness at the rim and the pit centre. This is illustrated in fig 2 as the difference between retinal thickness at plane A–E (rim height) and point C. The measured values of depth for each eye are an average of the measured depth for each of the six B-scans in the fast mac scan set. Other investigators have used a manual method to measure foveal pit depth, based on the distance between the temporal rim and the pit floor.[11]

The slope of the foveal pit is not constant. Here, we define foveal slope as the maximum slope of the foveal contour (points B andDin fig 2). Once the x-coordinate location of the minimum and maximum points were derived from $F'(x)$, the function $F'(x)$ was solved at these x-coordinates. The arc tangent was then taken to produce a slope value in degrees, and the absolute values were averaged. Measured values of slope for each eye are an average of the average slope for each of the six B-scans.

Three-dimensional model reconstruction—Custom Matlab programs were used to create a three-dimensional (3D) rendering of the retinal volume. Using the surf function, the six B-scans from a fast mac data set were combined to produce a 3D map of the fovea. To represent this foveal reconstruction, the shifted raw data sets were fitted to a two-dimensional (2D) DoG function (equation 3). These fits provided a qualitative picture of the fovea, though all foveal metrics were derived from the DoG fits to the individual B-scans, as DoG provides a better overall fit to the data than the 2D DoG. MatLab code for deriving foveal metrics/creating 3D renderings from .txt formatted thickness values is available upon request.

$$F(x,y)=A_1\times\left(\exp\left(\frac{(x-\mu_1)^2}{-2\sigma_1{}^2}\right)+\exp\left(\frac{(y-\mu_2)^2}{2\sigma_2{}^2}\right)\right)-A_2\times\left(\exp\left(\frac{(x-\mu_1)^2}{-2\sigma_3{}^2}\right)+\exp\left(\frac{(y-\mu_2)^2}{2\sigma_4{}^2}\right)\right)+z \quad (3)$$

RESULTS

Assessing model fit

The DoG (equation 1) fits the foveal contour extremely well (average root mean square (rms) error per B-scan = 141.22 (SD 23.24) μm; average error per A-scan is about 1 μm). For comparison, average rms error using a single Gaussian is about 300 μm per B-scan. However, some foveae have a slightly higher rim on the nasal side[13] due to the location of the papillomacular bundle heading from the fovea to the optic disc (located 4 mm nasal to the fovea[1]). Since the means of the two Gaussians are constrained to be equal, this difference will not be captured. Observations made in the data showed that the eye movements, defined by the position of the central point of the foveal pit, varied laterally about the mean at most by six A-scans (256 μm), and the average variation was 110 μm (just over two A-scans).

Measured pit characteristics

Measured parameters are given in table 1. We found significant inter-subject variability in all foveal metrics (depth, diameter and slope) in our sample; however, a high degree of

individual interocular symmetry was observed (Pearson r = 0.9185, 0.8735, 0.8621 for depth, diameter and slope, respectively; p<0.0001). Previous reports show that while on average there is symmetry in retinal thickness, there is potential for significant asymmetry in normal individuals.[14]

The average pit depth for the emmetropes was 122 (SD 20.2) μm. Pit depth was not statistically different between emmetropes and myopes ($t(59) = 1.502$, p = 0.1384; two-tail t test) or between emmetropes and BCM carriers ($t(41) = 1.103$, p = 0.2763; two-tail t test). The average pit diameter for the emmetropes subjects was 1.97 (SD 0.177) mm. Pit diameter was not statistically different between emmetropes and myopes ($t(59) = 0.5751$, p = 0.5674; two-tail t test). The BCM carriers had broader pits than the emmetropes, although this was not significant ($t(41) = 1.157$, p = 0.2538; two-tail t test). Pit slope was not statistically different between myopes and emmetropes ($t(59) = 1.478$, p = 0.1447; two-tail t test), nor between emmetropes and BCM carriers (t (41) = 1.759, p = 0.0861; two-tail t test). Previous reports in affected BCM men found significant thinning of the fovea,[15] although BCM carriers are generally unaffected, except for a possible reduction in cone-driven electroretinogram (ERG) amplitudes.[16]

Comparison with other OCT devices

Twenty-one subjects were imaged with both Zeiss OCT systems. Previous results have shown that Zeiss Stratus and Cirrus have a difference of 60 μm in total retinal thickness,[1718] as a result of an improvement in the assignment of the RPE layer within the outer hyper-reflective complex. This thickness difference would not be expected to affect our foveal metrics, as the difference in thickness between the two devices should be uniform across the retina and our measurements depend on relative, not absolute, differences in thickness.

In order to compare the data from the two devices, we analysed the simulated fast mac scan sets we created from the Cirrus volumetric scan set. As for the Stratus data, the DoG (equation 1) fits the Cirrus data extremely well (average rms error per B-scan = 141.49 (SD 38.57) μm). In comparing foveal metrics derived from the two systems, we found a significant correlation between measurements obtained using the two systems (table 2). Any systematic difference between the systems could be due to the fact that our correction for lateral shifts *between* scans does not account for eye movements *during* a single scan. In either case, the good correlation between metrics derived from the two systems indicates that it is possible to convert metrics derived from either system reliably.

In order to demonstrate that our algorithm can be applied to any OCT data set, we imaged one retina using the Bioptigen and Spectralis SD-OCT systems as well. Figure 3 shows topographical maps of the same retina obtained with four instruments. Foveal metrics were similar (within about 6%); for example, the pit diameters were 1.91, 1.85, 1.96 and 1.94 mm for the Stratus, Cirrus, Bioptigen and Spectralis data sets, respectively.

DISCUSSION

We developed an offline analytical technique to increase the utility of time-domain OCT. This can be used on existing OCT data sets, and could easily be modified for real-time analysis. One of the advantages of this analytical technique is that it is platform-independent and could be applied to any OCT data set (including SD-OCT), as long as one has access to retinal thickness data (or raw images from which thickness could be calculated or the difference between the ILM/RPE contours plotted). While SD-OCT technology has superior axial resolution and speed compared with time-domain systems,[19] both modalities capture foveal morphology equally well.

Time-domain OCT devices have permeated the ophthalmology and vision research communities and there is tremendous interest in the development of post-processing methods to expand the utility of these devices. For example, averaging multiple Stratus line scans from the same retinal location can be used to increase the signal to noise ratio. The resultant image quality is significantly improved, and these images can reveal subtle alterations of intraretinal architecture where individual scans cannot.[20] In addition, these high signal to noise time-domain images enable assessment of retinal lamination.[21] Bernardes *et al* (2008) modified existing scan protocols on the Stratus to improve the spatial resolution of retinal thickness maps by reducing the interpolation.[22] These studies, together with ours, illustrate how the clinical utility of time-domain devices (Stratus) could be improved through offline image processing. There is no doubt that SD-OCT offers superior image quality and resolution. However, given the abundance of time-domain systems and the significant cost associated with upgrading to SD-OCT, for some clinics the implementation of similar image processing techniques may prove to be a valuable, if not necessary, intermediate step.

We observed remarkable variation in foveal morphology across clinically normal individuals. It is somewhat difficult to make direct comparisons between the values presented here and those from previous studies. One of the main reasons is that we relied on automated data acquisition based on objective definitions of the various morphological features. For example, the diameters presented here represent the upper bound of typical measurements, which are often based on other features of the fovea, such as the avascular zone or rod-free region. A recent study by Hammer *et al* (2008) defined depth arbitrarily as the distance from base of the pit to the point where the radius is 0.728 μm.[8] Making the same measurement on our data we found no difference between the data sets, supporting the idea that any differences between our data and those of others rests solely on the definition of the foveal metrics used. Peak cone density in normal subjects can vary by a factor of three,[6] so future work will examine whether this variation is correlated with variation in gross foveal morphology, and how pit morphology compares with other anatomical landmarks, such as the rod-free region or the foveal avascular zone. Finally, normative data such as these should prove useful in quantitatively characterising clinically foveal hypoplasia/fovea plana.[23]

Acknowledgments

The authors thank J Rha, and J Kuchenbecker for helpful insights on mathematical modelling, T Connor Jr for valuable discussion, and A Gegios, N Ayub and J Beringer for assistance with imaging.

Funding: The authors acknowledge grant support from the National Institutes of Health (EY001931 and EY017607) and from the Posner Foundation, Fight for Sight, The E. Matilda Ziegler Foundation for the Blind, the RD & Linda Peters Foundation, and an unrestricted grant from Research to Prevent Blindness. J C is the recipient of a Career Development Award from Research to Prevent Blindness.

REFERENCES

1. Hendrickson, A. Organization of the adult primate fovea. In: Penfold, PL.; Provis, JM., editors. Macular Degeneration. Heidelberg: Springer-Verlag; 2005. p. 1-20.
2. Provis JM, Diaz CM, Dreher B. Ontogeny of the primate fovea: a central issue in retinal development. Prog Neurobiol. 1998; 54:549–581. [PubMed: 9550191]
3. Yuodelis C, Hendrickson A. A qualitative and quantitative analysis of the human fovea during development. Vision Res. 1986; 26:847–855. [PubMed: 3750868]
4. Hendrickson AE. Primate foveal development: a microcosm of current questions in neurobiology. Invest Ophthalmol Vis Sci. 1994; 35:3129–3133. [PubMed: 8045707]

5. Zeffren BS, Applegate RA, Bradley A, et al. Retinal fixation point location in the foveal avascular zone. Invest Ophthalmol Vis Sci. 1990; 31:2099–2105. [PubMed: 2211007]
6. Curcio CA, Sloan KR, Kalina RE, et al. Human photoreceptor topography. J Comp Neurol. 1990; 292:497–523. [PubMed: 2324310]
7. Williams DR. Visual consequences of the foveal pit. Invest Ophthalmol Vis Sci. 1980; 19:653–657. [PubMed: 7380624]
8. Hammer DX, Iftimia NV, Ferguson RD, et al. Foveal fine structure in retinopathy of prematurity: an adaptive optics fourier domain optical coherence tomography study. Invest Ophthalmol Vis Sci. 2008; 49:2061–2070. [PubMed: 18223243]
9. Springer AD, Hendrickson AE. Development of the primate area of high acuity. 1.Use of finite element analysis models to identify mechanical variables affecting pit formation. Vis Neurosci. 2004; 21:53–62. [PubMed: 15137581]
10. Springer AD, Hendrickson AE. Development of the primate area of high acuity. 2: Quantitative morphological changes assoicated with retinal and pars plana growth. Vis Neurosci. 2004; 21:775–790. [PubMed: 15683563]
11. Springer AD, Hendrickson AE. Development of the primate area of high acuity. 3: Temporal relationships between pit formation, retinal elongation and cone packing. Vis Neurosci. 2005; 22:171–185. [PubMed: 15935110]
12. Leung CK, Cheng ACK, Chong KKL, et al. Optic disc measurements in myopia with optical coherence tomography and confocal scanning laser ophthalmoscopy. Invest Ophthalmol Vis Sci. 2007; 48:3178–3183. [PubMed: 17591887]
13. Polyak, SL. The Retina. Chicago: University of Chicago Press; 1941.
14. Huynh SC, Wang XY, Burlutsky G, et al. Symmetry of optical coherence tomography retinal measurements in young children. Am J Ophthalmol. 2007; 143:518–520. [PubMed: 17317402]
15. Barthelmes C, Sutter FK, Kurz-Levin MM, et al. Qualitative analysis of OCT characteristics in patients with achromatopsia and blue-cone monochromatism. Invest Ophthalmol Vis Sci. 2006; 47:1161–1166. [PubMed: 16505054]
16. Berson EL, Sandberg MA, Maguire A, et al. Electroretinograms in carriers of blue cone monochromatism. Am J Ophthalmol. 1986; 102:254–261. [PubMed: 3488684]
17. Durbin, M.; Abunto, T.; Chang, M., et al. [accessed 10 June 2009] Retinal measurements: comparison between Cirrus HD-OCT and Stratus OCT. http://www.zeiss.com/C125679E00525939/EmbedTitelIntern/cirruswhitepaper/$File/cirrus_whitepaper.pdf
18. Kakinoki M, Sawada O, Sawada T, et al. Comparison of macular thickness between Cirrus HD-OCT and Stratus OCT. Ophthalmic Surg Lasers Imaging. 2008; 39:S37–S42.
19. Drexler W. Ultrahigh-resolution optical coherence tomography. J Biomed Optics. 2004; 9:47–74.
20. Sander B, Larsen M, Thrane L, et al. Enhanced optical coherence tomography imaging by multiple scan averaging. Br J Ophthalmol. 2005; 89:207–212. [PubMed: 15665354]
21. Christensen UC, Kroyer K, Thomadsen J, et al. Normative data of outer photoreceptor layer thickness obtained by software image enhancing based on Stratus optical coherence tomography. Br J Ophthalmol. 2008; 82:800–805. [PubMed: 18523085]
22. Bernardes R, Santos T, Cunha-Vaz J. Increased-resolution OCT thickness mapping of the human macula: a statistically based registration. Invest Ophthalmol Vis Sci. 2008; 49:2046–2052. [PubMed: 18436839]
23. Marmor MF, Choi SS, Zawadzki RJ, et al. Visual insignificance of the foveal pit. AMA Arch Ophthalmol. 2008; 126:907–913.

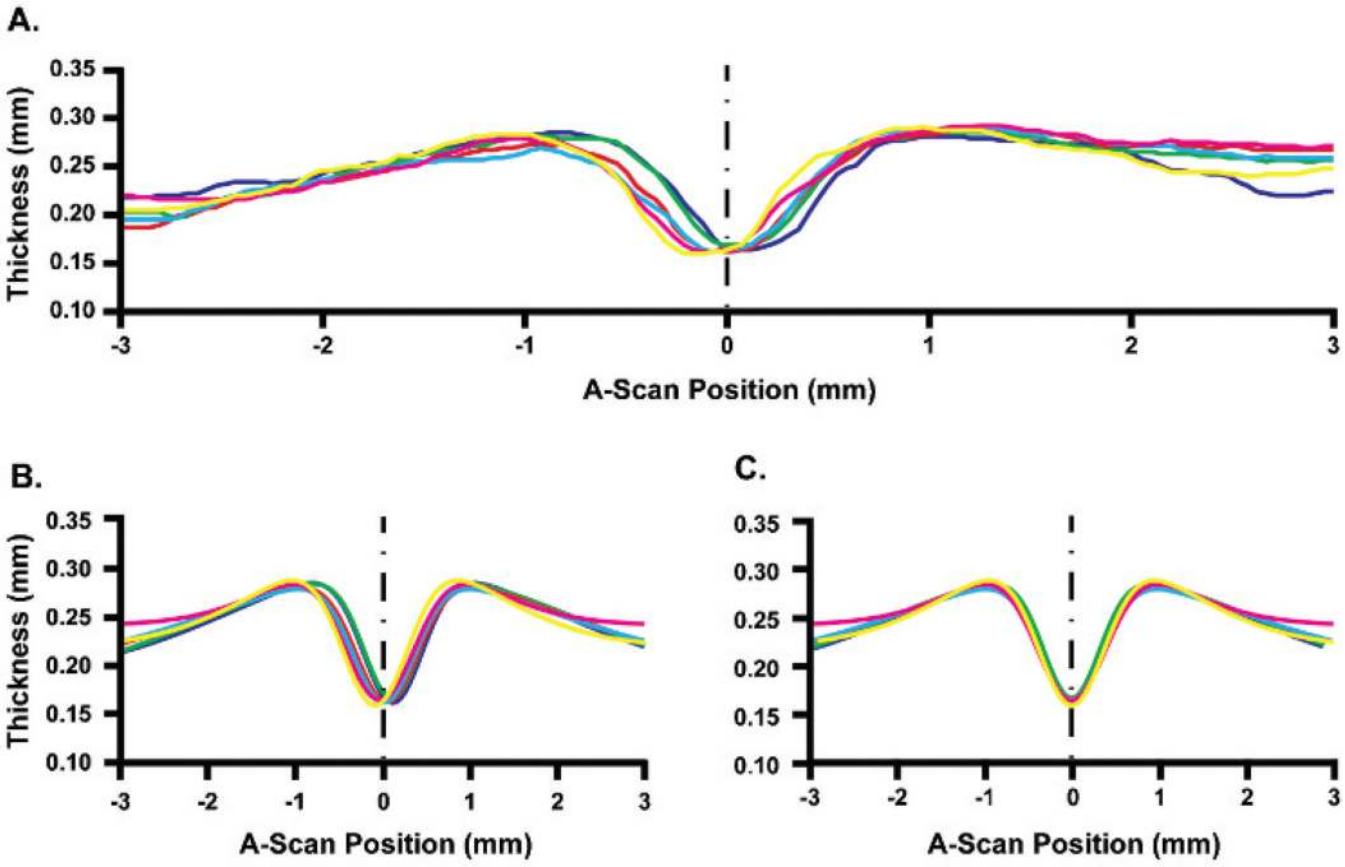

Figure 1.

Fitting and shifting individual line scans from a radial scan set. (A) A representative sample of raw data from the six individual B-scans (at 128 A-scans/B-scan), rotated for plotting in the same two-dimensional plane. This data were then fitted to a difference of Gaussian (DoG) equation; the resulting best fits to these six line scans are shown in (B). Lateral shifts in the data, due to eye movements between scans, were then calculated for each scan. These corrected scans are shown in panel (C). This correction brings all scans to the same centre, which can be thought of as an empirically defined foveal centre.

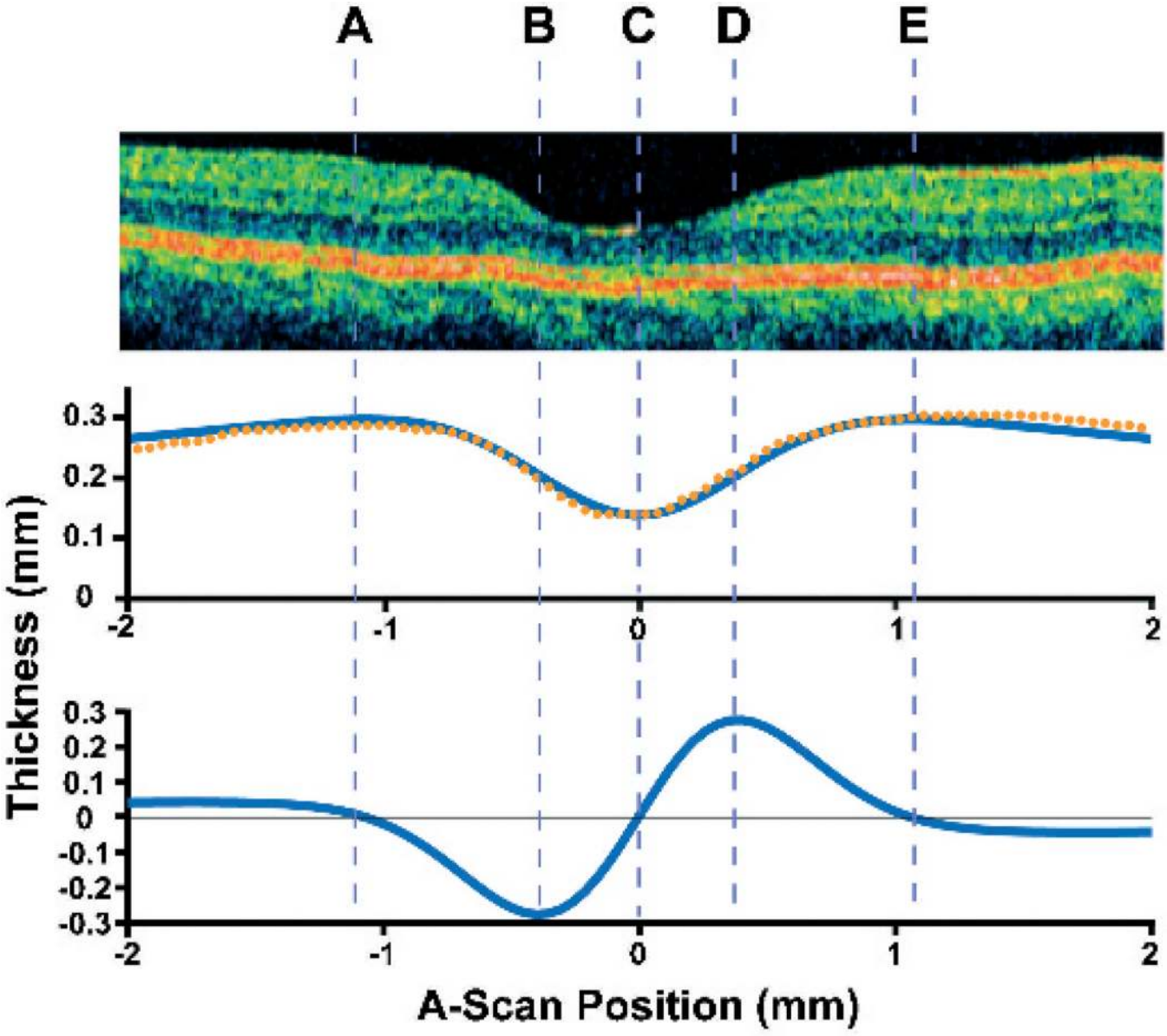

Figure 2.

Foveal parameters are derived from specific locations with in the scan. The top panel shows a 4 mm section of an individual line scan from the Stratus system. The middle panel shows a plot of the raw thickness data for this scan (filled circles) and the difference of Gaussian (DoG) fit to the data (solid line). The bottom panel shows the first derivative of this DoG fit. Drawn through these plots are lines A–E, corresponding to objectively defined anatomical landmarks (see text).

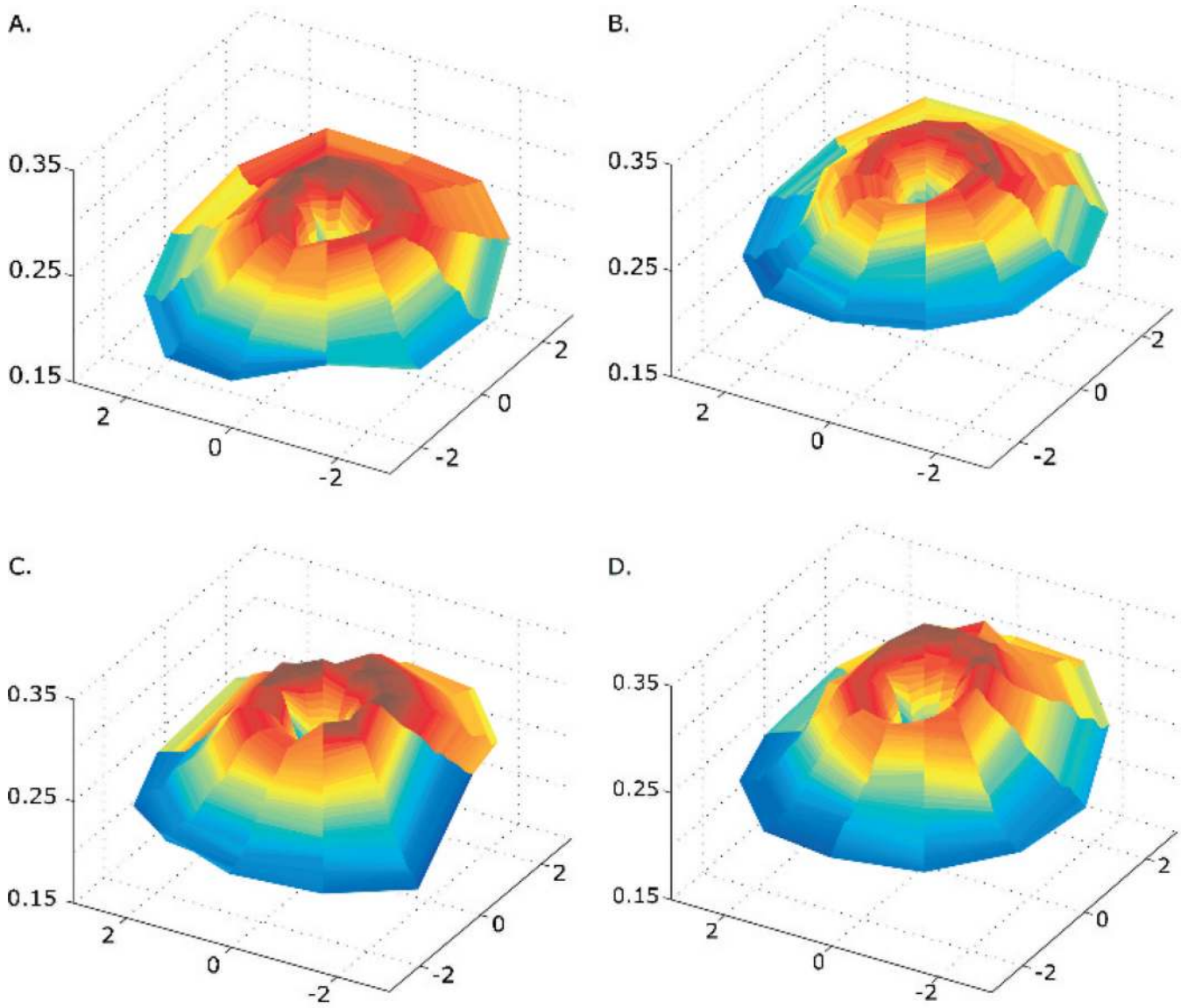

Figure 3.

Maps of foveal morphology from four different optical coherence tomography instruments. (A) Three-dimensional representation of the retinal thickness derived from a Stratus "fast mac" data set from a normal subject. (B) From the same subject, a thickness map from a Cirrus 512 × 128 volumetric macular scan, where six lines scans at 30° increments were obtained, with points interpolated from the neighbouring three points when needed, generating the Cirrus equivalent of a fast mac scan. (C) From the same subject, a thickness map from a Bioptigen radial scan profile, where six lines at 30° increments were collected. (D) From the same subject, a thickness map from a Spectralis radial scan profile, where six lines at 30° increments were collected using the Eye Tracking ART™ feature. Increased "noise" in the Bioptigen and Spectralis data reflects the fact that the inner limiting membrane and retinal pigment epithelium layers were manually picked. Nevertheless, all four devices offer automated representation of the retinal thickness, regardless of how the thickness data were obtained, and objective assessment of pit morphology. Differences in total thickness between time-domain (A) and spectral-domain (B–D) images are consistent

with previous reports indicating a 60 μm difference between Stratus and spectral-domain instruments.[1213] Axes for all panels are shown in mm.

Table 1

Comparison of foveal metrics derived from Stratus optical coherence tomography images for emmetropes, myopes and carriers of blue-cone monochromacy

	Emmetropes (n = 39)	Myopes (n = 22)	BCM carriers (n = 4)
Depth (μm)	122.53 (3.2)	112.5 (6.8)	110.7 (11.0)
Diameter (mm)	1.972 (0.029)	1.943 (0.044)	2.078 (0.066)
Slope (°)	12.241 (0.32)	11.299 (0.63)	10.407 (0.92)

Values are means with standard error of the mean.

BCM, blue-cone monocromacy.

Table 2

Comparison of foveal metrics derived from Stratus and Cirrus optical coherence tomography images from 21 subjects

	Stratus	Cirrus	Correlation*	p Value
Depth (μm)	113.5 (5.6)	112.5 (6.0)	0.9411	<0.0001
Diameter (mm)	1.905 (0.049)	1.912 (0.056)	0.8202	<0.0001
Slope (°)	12.157 (0.52)	11.705 (0.54)	0.8004	<0.0001

Values are means with standard error of the mean.

*Pearson r correlation coefficient.